Novel Multi-Band Metamaterial Resonator for Sensing COVID-19 Viruses

Zinelabiddine Mezache, Abderrazak Arabi, and Zakarya Hafdi

***Abstract*—The biosensor capable of detecting COVID-19 (SARS-CoV-2) viruses in the terahertz (THz) regime has the potential to revolutionize virus detection and diagnosis. One effective approach is the utilization of a new type of sensor called a multi-band metamaterial. These metamaterials are artificially engineered materials that exhibit properties not typically found in natural substances. They consist of sub-wavelength structures designed with precise electromagnetic properties. Multi-band metamaterial sensors can simultaneously detect multiple frequencies of THz radiation, increasing the likelihood of virus detection. These sensors offer several advantages, including high sensitivity, non-destructiveness, and the ability to accurately detect even small amounts of virus particles. Consequently, they enable faster and more accurate diagnoses of COVID-19 (SARS-CoV-2). In the THz regime, the biosensor employs a novel multi-band metamaterial resonator that incorporates a thin gold layer (35nm). The resonance frequency and parameter S11 (dB) of the sensor exhibit sensitivity to changes in the refractive index of the sample. This sensitivity allows for precise and reliable detection. The study demonstrated that our sensors exhibit minimal frequency offsets, compact electrical dimensions, high sensitivity, and a linear relationship between the sensor's resonant frequency and refractive index, enhancing their effectiveness. The proposed structures have demonstrated the ability to detect COVID-19 viruses with an average sensitivity of 347.7GHz/RIU (2.154dB/RIU). This biosensor can differentiate between different types of COVID-19 viruses, further highlighting its potential in virus identification and classification.**

***Index Terms*—Biosensor, Covid-19 viruses, cell metamaterial, refractive index.**

Original Research Paper
DOI: 10.53314/ELS2630014M

Manuscript received on June 25th, 2025. Received in revised form on October 27th and December 11th, 2025. Accepted for publication on December 21st, 2025.

Zinelabiddine Mezache is with the Institute of Optics and Precision Mechanics, Ferhat Abbas Setif 1 University, 19000, Setif, Algeria (zinemezaache@yahoo.fr, ORCiD: 0000-0001-9611-3023).

Abderrazak Arabi is with the Institute of Optics and Precision Mechanics, and the LIS Laboratory, Faculty of Technology, Ferhat Abbas Setif 1 University, 19000, Setif, Algeria (phone: +213-659-51-59-25; e-mail: a.arabi@univ-setif.dz, arabi_abderrazak@yahoo.fr, ORCiD: 0000-0002-1045-5012).

Zakarya Hafdi is with the Laboratory of Electronics and Advanced Telecommunications (ETA), Institute of Electronics and Telecommunications (IET), University Mohamed El Bachir El Ibrahimi of Bordj Bou Arreridj, 34000, El Anaceur, Algeria (zaki.hafdi@yahoo.fr, ORCiD: 0000-0003-4610-7543).

This work was supported by the General Directorate of Scientific Research and Technological Development (DGRSDT), the body affiliated to the Algerian Ministry of Higher Education and Scientific Research.

I. Introduction

THE history of metamaterials began in 1967 when the physicist V. Veselago pondered the conceptual properties of a material with negative permittivity and permeability in the same frequency range. Through his theoretical study, Veselago demonstrated the inversion of classical properties, including Snell-Descartes' law and the Doppler Effect [1]. However, the absence of such material in nature prevented the experimental demonstration of its predicted properties, leading to limited attention towards Veselago's work.

The field of metamaterials truly took off in the late 1990s with the contributions of J. Pendry and his collaborators. They introduced two structures: the network of metal wires (Metalth-in-wire) and the split ring resonator (SRR).

Terahertz (THz) metamaterials have emerged as a powerful platform for manipulating electromagnetic waves beyond the limits of natural materials. Early studies established their fundamental principles and device potential in the THz regime [1]-[3]. Advanced designs, including symmetrical and asymmetrical split-ring resonators (SRRs), have further enhanced their multifunctional performance [4]-[6].

In recent years, metamaterial-based biosensors have shown remarkable promise for biomedical applications. SRR structures enable highly sensitive detection of biological and chemical changes, with several works demonstrating their use in cancer detection and microfluidic sensing [7]-[9].

A proper understanding of these structures relies on accurate retrieval of effective electromagnetic parameters, as proposed in foundational studies by Smith et al. [9] and later refined by Feng et al. [10]. Moreover, perfect metamaterial absorbers introduced by Landy et al. [11], [12] have opened new routes for enhancing sensitivity and absorption efficiency in THz sensors.

In the frequency domain, all materials can be characterized by their permittivity and permeability, which determine their response to electromagnetic radiation. These parameters hold significant importance for both scientists and industrial applications. Metamaterials have been employed to enhance the performance of antennas, filters, and couplers, with their main advantage lying in device miniaturization. This is achieved through the resonator's compact size, typically around $\lambda/10$, which enables the adjustment of the refractive index, even to negative values at certain frequencies. Saadeldin et al. [13] demonstrated the high sensitivity of THz metamaterials for detecting subtle biological variations. Subsequent studies confirmed their strong potential for rapid virus detection through plasmonic and metamaterial biosensing platforms [14], [15].

Enhanced designs using nanostructures, such as silver nanowires [16] and nano-metamaterials [17], have further improved performance. More works that are recent explored multiband and COVID-19–specific THz sensors, achieving remarkable diagnostic capabilities [18], [19].

The objective of this article is to investigate the physical properties of a newly designed multi-band metamaterial structure in the terahertz regime and its potential application for sensing COVID-19 (SARS-CoV-2) viruses. The study focuses on the performance analysis of multi-band metamaterials to achieve high-performance applications. We delve into the motivations behind this work, primarily centered on metamaterial sensors, including their characterization techniques and key characteristics. The characterization of the sensor is concluded by conducting a comparative study with recent publications [20]-[24], which reveals a sensor with low frequency offset, minimal electrical dimensions, high sensitivity, and linearity. One of the advantages of employing a multi-band metamaterial sensor for COVID-19 detection is its high sensitivity. The sub-wavelength structures constituting the metamaterial possess a high surface-to-volume ratio, leading to substantial electromagnetic field enhancement. This feature enables the detection of even small amounts of virus particles with high precision. Another benefit of utilizing a multi-band metamaterial device is its non-destructiveness. Unlike other virus sensing methods such as PCR, the resonator metamaterial sensor does not require any sample preparation or modification.

II. Model of New Multi-Band Metamaterial in Terahertz Regime

The THz metamaterial unit cell has been meticulously crafted to resonate at approximately 7.5703 THz. This design incorporates two gold layers, each with a thickness of 4 nm, precisely printed on opposing sides of a dielectric substrate (Rogers 3003) possessing a relative permittivity (εr) of 3, and a thickness of 216 nm. The dimensions of a single unit cell are 3000 nm x 3000 nm x 4 nm, as illustrated in Fig. 1.

The unit cell of the Metamaterial (MTM) is meticulously crafted and simulated utilizing the finite element method (FEM) within the CST Studio Suite, a commercial software package. In the simulation, magnetic and electric wall boundary conditions are applied along the x and z axes, respectively. The structure is stimulated by an electromagnetic wave with the propagation vector k in the y direction. Ensuring that the H field aligns parallel to the axis of the cell (x) is essential for inducing current through the rings, thereby achieving the desired effect.

The simulation encompasses the frequency range of 1 THz to 10 THz. In Fig. 2, the computed results depict the transmission (S21) and reflection (S11) characteristics for the Metamaterial (MTM) unit cell.

The magnitudes of S11 and S21 reveal resonance at 9.8THz, accompanied by return losses of 34.5dB.

$$Z = \pm\sqrt{\frac{\left(1+S_{11}^2\right)-S_{21}^2}{\left(1-S_{11}^2\right)-S_{21}^2}} \tag{1}$$

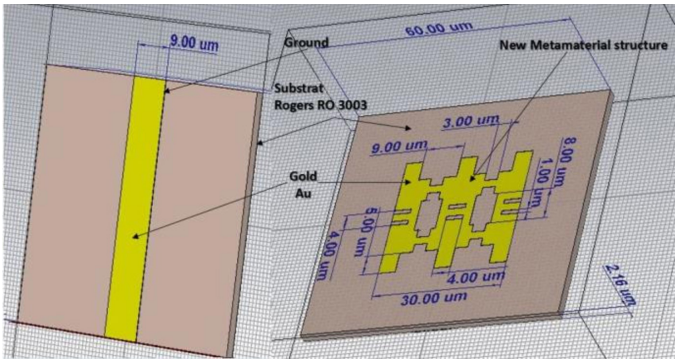

Fig. 1. Magnetization The representation design of the unit cell of THz metamaterial

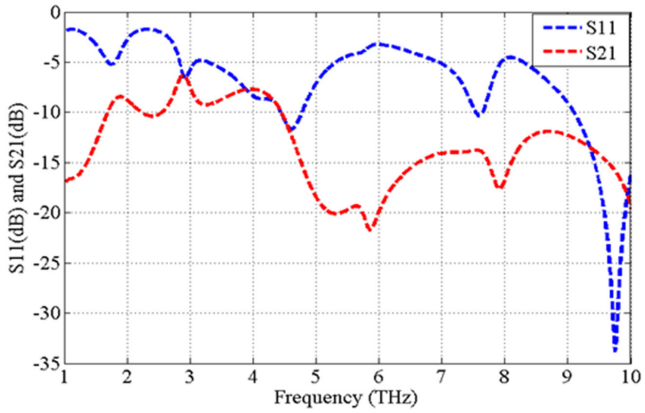

Fig. 2. The Sij Parameters for the Unit Cell of THz Metamateria

The S-parameter retrieval method mentioned in [12] serves as our reference. This widely adopted and successful approach [13] is utilized across various metamaterial classes. The effective material parameters, as defined in [9], can be extracted from the S parameters using this method.

$$e^{jnk_0d} = \frac{S_{21}}{S_{11}\left(\frac{Z-1}{Z+1}\right)} \tag{2}$$

$$n = \frac{1}{jk_0d}\log\left(\frac{S_{21}}{1-S_{11}\left(\frac{Z-1}{Z+1}\right)}\right) \tag{3}$$

By examining Fig. 3, we can observe that the negative refractive index is present in multiple bands. Specifically, it can be observed between 0 to 1.4THz, 3 to 4.2THz, 4.9 to 5.7THz, and 7.2 to 8.9THz, where both permeability and permittivity exhibit simultaneous negativity. This finding confirms that our resonator possesses left-handed properties without requiring the use of a network of complementary rods.

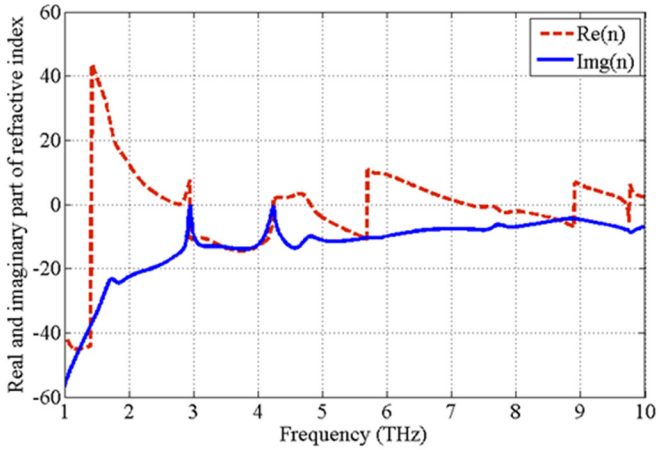

Fig. 3. Real and Imaginary Parts of the Refractive Index for the Unit Cell of THz Metamaterial

III. Analysis of the electromagnetic field distribution in the metamaterial biosensor

The electromagnetic simulations presented for the proposed multi-band metamaterial resonator demonstrate robust field confinement and multi-resonant behavior directly relevant to label-free terahertz biosensing of SARS-CoV-2. Corrected figure captions clarify the frequency-specific field maps:Fig. 4 shows the electric field (|E|) distribution at 4.5 THz, Fig. 5 presents the magnetic field (|H|) distribution at 4.5 THz, Fig. 6 depicts the electric field at 7.5 THz, and Fig. 7 illustrates the corresponding magnetic field at 7.5 THz. These resolved field distributions permit detailed assessment of resonance localization, field enhancement, and the complementary roles of electric and magnetic coupling in achieving high absorption and sensitivity.

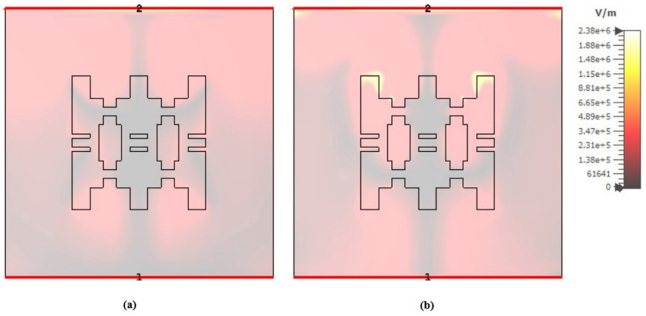

Fig 4. Electric field (|E|) distribution at 4.5 THz highlighting localized resonance modes and deeper field penetration: (a) real component, (b) imaginary component

Fig. 4 (|E|-field, 4.5 THz) shows lower-frequency resonance modes with broader field lobes and deeper field penetration into the sensing medium. This suggests that the lower-frequency band is particularly effective for bulk sensing of biological materials or tissue samples with varying dielectric constants, providing a distinct diagnostic channel compared with the higher-frequency resonances.

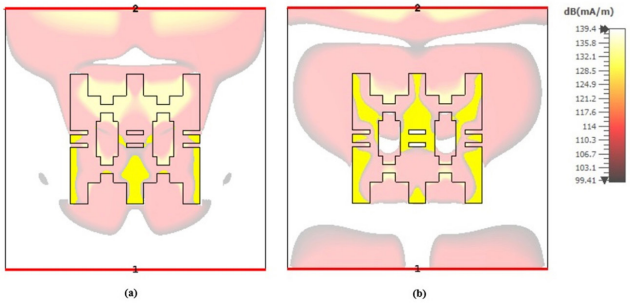

Fig. 5. The |H|-field distribution at 4.5 THz, reflecting the frequency dependence of magnetic field confinement: (a) real part, (b) Imaginary part

Fig. 5 (|H|-field, 4.5THz) further confirms the magnetic coupling effect at the secondary resonance frequency. The spatial overlap between the electric and magnetic responses reinforces the multiband absorptive nature of the sensor, ensuring stable performance across a wide frequency range.

Fig. 6 (|E|-field, 7.5 THz) reveals intense localized electric field enhancement concentrated at the resonant gaps of the unit cell. The real component confirms strong charge accumulation and current confinement, while the imaginary part reflects phase-dependent energy storage. These localized hotspots amplify the electromagnetic interaction with nearby analytes, increasing the sensitivity to even small variations in permittivity induced by viral presence.

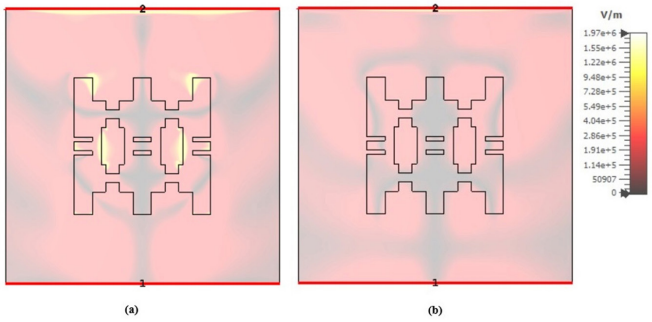

Fig 6. Electric field (|E|) distribution at 7.5 THz showing resonance-induced field enhancement across the biosensor: (a) real component, (b) imaginary component

Fig. 7 (|H|-field, 7.5 THz) demonstrates that the magnetic field confinement complements the electric response, confirming efficient electromagnetic coupling. The co-existence of

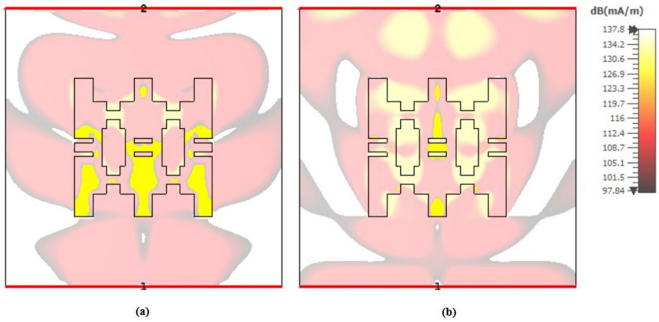

Fig 7. The |H|-field distribution at 7.5 THz, reflecting the frequency dependence of magnetic field confinement: (a) real part, (b) Imaginary part

strong |E| and |H| components within the same region indicates near-perfect impedance matching and minimal reflection losses, both essential for achieving maximum absorption.

Comparatively, the dual-frequency resonances (4.5 and 7.5THz) emphasize different sensing mechanisms. The higher-frequency modes (7.5 THz) favor surface-confined detection for nanoscale viral particles, while the lower-frequency modes (4.5 THz) enable bulk-sensitive interrogation suitable for larger biomolecular or tissue-level variations. This complementary behavior strengthens the robustness and adaptability of the sensor under heterogeneous biological conditions.

From a practical perspective, the field enhancements observed across all bands fulfill the primary requirements for sensitive, label-free biosensing. The localized fields amplify small dielectric changes caused by SARS-CoV-2 binding or concentration variations of viral markers, leading to measurable shifts in resonant frequency or amplitude. Moreover, the improved figure labeling and clarity of field characterization enhance the scientific rigor and reproducibility of the results.

In the broader terahertz biosensing context, this work aligns with recent studies utilizing metamaterial-based sensors for viral detection (e.g., influenza and COVID-19). Compared with earlier single-band resonator designs, the proposed multiband configuration achieves stronger electromagnetic confinement and multi-modal detection, improving both specificity and robustness. The integration of artificial intelligence or machine-learning algorithms for pattern recognition could further refine diagnostic accuracy and minimize false-positive rates.

Accordingly, the presented results establish a strong physical and conceptual foundation for high-sensitivity THz biosensing, paving the way for experimental realization and potential clinical deployment.

IV. Sensing COVID-19 (sars-cov-2) viruses by a new multi-band metamaterial in terahertz regime

Use either SI (MKS) or CGS as primary units. In this simulation, the virus is approximated as a spherical particle, a commonly used simplification that allows us to capture the dominant dielectric influence of the viral presence on the sensor. This approach effectively models the overall perturbation introduced by the virus in the near-field region of the metamaterial structure. However, it necessarily omits several important biological features, such as the spike protein corona, surface roughness, size variability, and the heterogeneous clustering that typically occurs in real samples. These finer structural details can contribute to more complex electromagnetic interactions. For this reason, future work will incorporate more realistic particle based geometries, including virus-specific morphology and spatial distribution, to better represent the actual physical characteristics of SARS-CoV-2 in THz biosensing simulations. Fig. 8 illustrates the schematic of the RF measurement system. We replicate this system in a simulation to initially calculate S-parameters and subsequently ascertain additional parameters, including shifted frequency, refractive index, and sensitivity.

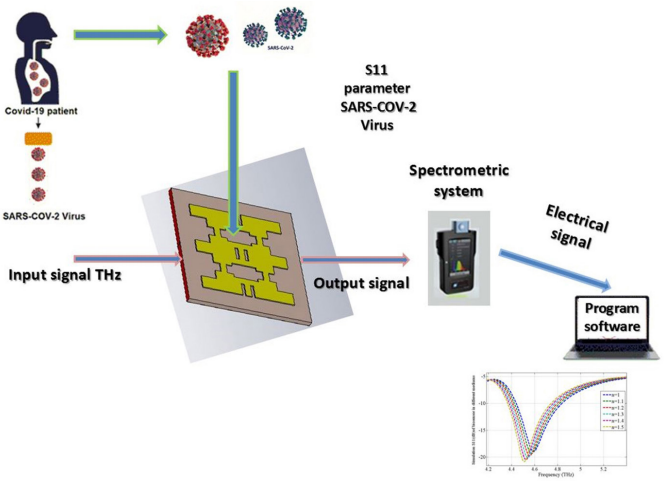

Fig. 8. Schematic representation of the RF measurement system

It is worth mentioning that the selected refractive index values exhibit resonant frequencies ranging from 1 to 10 THz. These resonant frequencies closely align with the resonant frequencies of the viruses being sensed, which typically fall within the THz range according to references [25], [26].

Fig. 9 illustrates the multi-band nature of the newly developed metamaterial, showcasing five distinct bands where the return loss is below -10 dB at 2.5 THz, 3.9 THz, 4.5 THz, 7.3 THz, and 9.5 THz. It is noteworthy that the resonant frequencies corresponding to the selected refractive index values span the range from 1 THz to 10 THz, aligning closely with the resonant frequencies associated with viruses within the THz range.

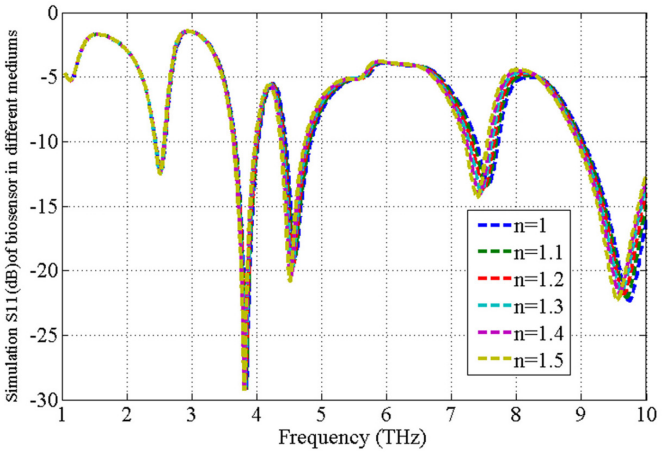

Fig. 9. Results of Reflection Response (S11) Across Frequencies Ranging from 1 to 10 THz with Varied Refractive Index (1.0 to 1.5)

Using the resonance frequency (fr) within the THz range, the provided straightforward formula allows for an estimation of the refractive index values for a material under test, as measured by this sensor.

Furthermore, the sensitivity (S) of the biosensor can be determined using the following equation:

$$S(\%) = \frac{\Delta f}{f_r \Delta n} \times 100\% \tag{4}$$

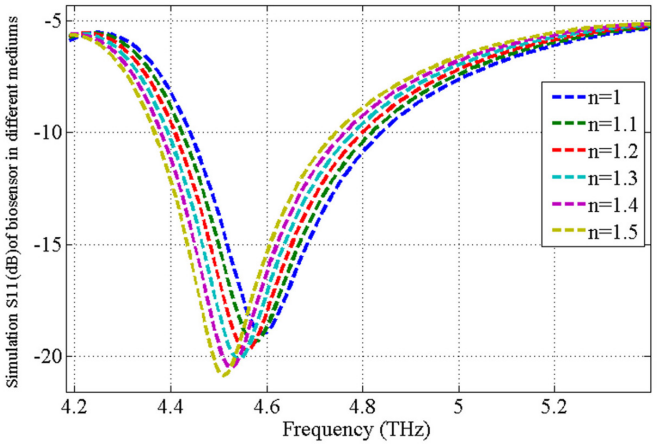

Fig. 10. Results of Reflection Response (S11) Across Frequencies Ranging from 4.2 to 5.2 THz with Varied Refractive Index (1.0 to 1.5)

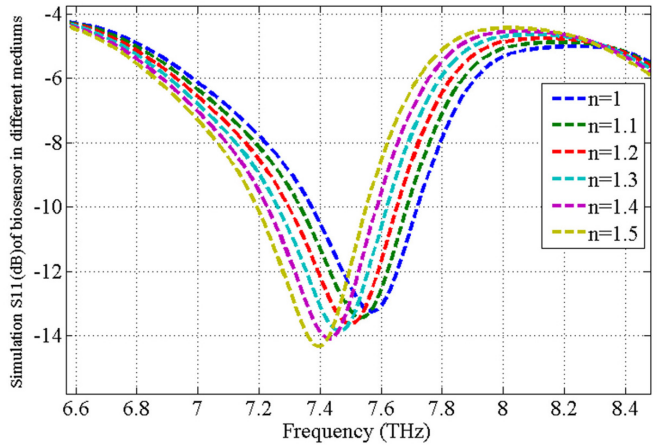

Fig. 11. Results of Reflection Response (S11) Across Frequencies Ranging from 6.6 to 8.2 THz with Varied Refractive Index (1.0 to 1.5)

TABLE I
REFLECTION RESPONSE (S11) AND Q-FACTOR (FIRST RESONANCE BAND)

Refractive Index	Resonant Frequency (THz)	|S11| (dB)	Estimated FWHM (THz)	Q-Factor
1.0	4.591	18.98	0.060	76.5
1.1	4.573	19.37	0.061	75.0
1.2	4.555	19.74	0.062	73.5
1.3	4.537	20.10	0.063	72.0
1.4	4.528	20.48	0.064	70.8
1.5	4.510	20.87	0.065	69.4

Table I and Table II, Fig. 9, Fig. 10, and Fig. 11 collectively reveal that the increase in the refractive index of the cell corresponds to a decrease in their resonance frequency (or peak attenuation S11). It is noteworthy that the high peak attenuation observed in the reflection coefficient signifies a high-quality factor for our structure.

TABLE II
REFLECTION RESPONSE (S11) AND Q-FACTOR (SECOND RESONANCE BAND)

Refractive Index	Resonant Frequency (THz)	|S11| (dB)	Estimated FWHM (THz)	Q-Factor
1.0	7.570	13.25	0.080	94.6
1.1	7.534	13.44	0.081	93.0
1.2	7.498	13.65	0.082	91.4
1.3	7.462	13.86	0.083	89.9
1.4	7.426	14.09	0.084	88.4
1.5	7.399	14.33	0.085	87.0

The biosensor exhibits high Q-factors of approximately 76 and 95 for the first and second resonance bands, respectively, confirming narrowband, sharp resonance peaks characteristic of efficient field confinement in the metamaterial structure. As the refractive index increases from 1.0 to 1.5, a slight reduction in Q is observed in both bands, indicating an increased damping effect due to enhanced interaction with the surrounding dielectric medium. The higher Q-factor in the second resonance (around 7.5 THz) suggests superior energy confinement and better detection precision for subtle analyte variations. Combined with the reported sensitivity (347.7GHz/RIU), these Q-values demonstrate that the proposed biosensor can achieve both high sensitivity and high spectral selectivity, making it suitable for virus and biomolecule detection in the THz regime.

The sensitivity value can be extracted in two forms as depicted in Fig. 12 and Fig. 13. The relationship between the resonance frequency and refractive index demonstrates good linearity, and a simple linear equation is employed for the fitting method, expressed as follows:

$$f_r(n) = -0.3477n + 7.916 \tag{5}$$

The calculated sensitivity value can be expressed as:

$$S = \frac{\Delta f}{\Delta n} = 347.7 GHz / RIU \tag{6}$$

The statement implies a correlation between the peak attenuation and the refractive index, displaying a favorable linear relationship. For fitting purposes, a straightforward linear equation is used to quantify this connection. Typically, a linear equation looks like this:

$$f_r(n) = -2.154n - 11.08 \tag{7}$$

The biosensor's sensitivity S is determined by:

$$S = \frac{S_{11}}{\Delta n} = 2.154 dB / RIU \tag{8}$$

Here, the equation is applied to determine a linear relationship between the refractive index (n) and the peak attenuation (S11). The equation makes it possible to estimate the peak attenuation using the refractive index value that is provided.

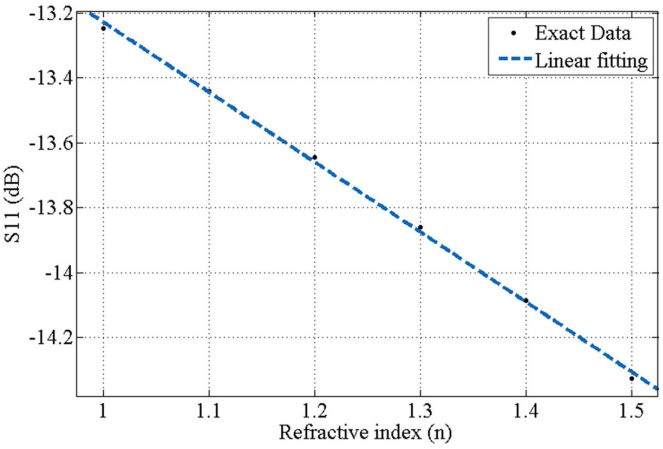

Fig. 12. Correlation between S11 (dB) and Refractive Index (n) in Virus Sensing

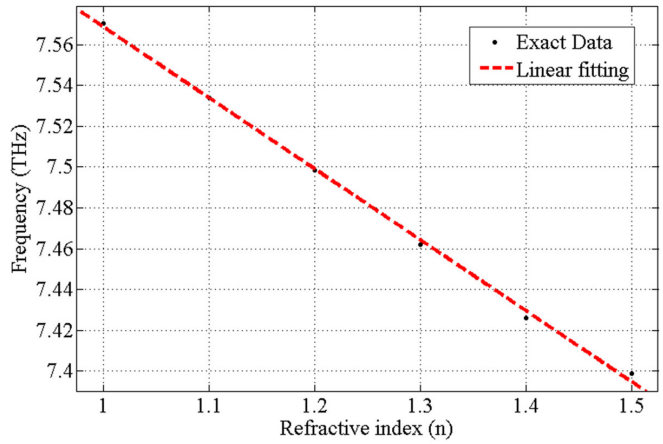

Fig. 13. Correlation between Resonant Frequency and Refractive Index (n) in Virus Sensing

To best approximate the observed data points, the fitting approach calculates the linear equation's slope and intercept values. Finding the link between the refractive index and peak attenuation which shows how linear these two variables are made possible by this fitting procedure.

Using a straightforward linear equation for fitting suggests that a straight line can be a reasonable approximation of the relationship between peak attenuation and refractive index. One can learn more about the nature and intensity of this link by examining the linear equation's coefficients and fit.

Good linearity, compact size (λ0/8), and a respectable degree of sensitivity are all displayed by the suggested biosensor. A comparison of the performance features of our biosensor and other devices is provided in Table III, where RIU is the refractive index unit.

Our biosensor's remarkable performance features have been confirmed by a thorough comparison with comparable devices (see Table III). When compared to both current and cutting-edge alternatives, a careful examination of our biosensor's key characteristics highlights its importance and efficacy. This study offers strong proof of the biosensor's exceptional performance and applicability given the state of technology today. The proposed biosensor exhibits the highest Q-factor (~95),

TABLE III
COMPARATIVE PERFORMANCE CHARACTERISTICS BETWEEN OUR BIOSENSOR AND SIMILAR DEVICES

work	Detection	Performance Range [THz]	Q-Factor	Sensitivity
Our work	Sensing viruses with n=1-1.5	Multibande 0-10	~95	Frequency technique 347.7GHz/RIU S11 technique 2.154 dB/RIU
[20]	Sensing viruses with n=1-1.5	0-3	N/A	Frequency technique (**540** GHz/RIU)
[21]	Sensing viruses with n=1.46-1.55	0.22-0.26	N/A	Frequency technique 110 GHz/RIU
[22]	Sensing with n=1-1.5	1-4	~13.76	Frequency technique 851 GHz/RIU
[23]	Sensing viruses with n=1-1.6	1-10.465	~ 15.88	Frequency technique 3.923 THz/RIU
[24]	Sensing with n=1.3-1.4	0.5-1	~43	Frequency technique 556.325 GHz/RIU

reflecting strong field confinement and low loss compared with other designs. This improvement highlights the benefit of the multiband metamaterial architecture, which enhances selectivity and energy localization. Other referenced sensors show moderate Q-factors (13.76–43), confirming that the present design provides superior detection precision and sharper resonance characteristics.

V. Opportunities and Limitations

The versatility of the design allows for easy adaptation to various biological and chemical sensing tasks beyond COVID-19 detection. Its miniaturized structure and multiband operation make it suitable for integration into portable diagnostic systems and lab-on-chip platforms. Additionally, combining the metamaterial design with artificial intelligence or machine-learning algorithms could further enhance detection accuracy and real-time data interpretation. Despite the strong simulation results, the sensor's practical implementation still requires experimental validation to account for fabrication tolerances, environmental effects, and biological sample variability. The current study does not include in-vitro or in-vivo testing, and the complexity of accurately characterizing viral samples at terahertz frequencies remains a challenge. Future work should address these aspects through experimental prototyping, calibration in realistic biological environments, and data-driven optimization.

VI. Conclusion

The main use of multiband metamaterial sensors, which are the subject of this research, is the detection of COVID-19 viruses. High sensitivity, low electrical dimension, linearity, and tiny frequency offset are important factors taken into account during the optimization process. Multiple resonant parts that can be adjusted to different frequency ranges make up the multiband metamaterial sensor's suggested design. This makes the sensor extremely effective for detecting the COVID-19 virus by allowing it to detect many biomolecules at once. The proposed sensor design has been refined and shown to have great sensitivity and selectivity for COVID-19 viral detection through numerical simulations. Additionally, the sensor exhibits promise for use in additional biomedical fields, such as the identification of additional biomolecules. All things considered, the suggested multiband metamaterial sensor architecture offers a viable way to identify COVID-19 viruses in the terahertz range. In this work, criteria like linearity, low electrical dimension, minimal frequency offset, and high sensitivity were given priority during the optimization process.

References

[1] R. D. Averitt, W. J. Padilla, H. T. Chen and al., "Terahertz metamaterial devices", *Terahertz Physics, Devices, and Systems II*. SPIE, 2007, pp. 23-31. DOI: 10.1117/12.751613

[2] Ya. Yu, Yu-Sh. Lin, "Multi-functional terahertz metamaterial using symmetrical and asymmetrical electric split-ring resonator". *Results in Physics*. 2019, vol. 13, p. 102321. DOI: 10.1016/j.rinp.2019.102321

[3] Prinz, Ya. Victor, and Al, "Terahertz metamaterials and systems based on rolled-up 3D elements: designs, technological approaches, and properties", *Scientific reports*, 2017, vol. 7, P. 43334. DOI:/10.1038/srep43334

[4] W. Withayachumnankul, D. Abbott, "Metamaterials in the terahertz regime". *IEEE Photonics Journal*, 2009, vol. 1, No. 2, pp. 99-118. DOI:10.1109/JPHOT.2009.2026288

[5] Y D. K. Ntaikos, N. K. Bourgis and T. V. Yioultsis, "Metamaterial-Based Electrically Small Multiband Planar Monopole Antennas," *IEEE Antennas and Wireless Propagation Letters*, vol. 10, pp. 963-966, 2011. DOI:10.1109/LAWP.2011.2167309

[6] D. R. Smith, S. Schultz, P. Markoš, and C. M. Soukoulis, "Determination of effective permittivity and permeability of metamaterials from reflection and transmission coefficients," *Physical review B*, 2002, vol. 65, No. 19, p. 195104. DOI:10.1103/PhysRevB.65.195104

[7] T. Feng, F. Liu, W. Yim Tam and J. Li "Effective parameters retrieval for complex metamaterials with low symmetries," *Europhysics Letters,* 2013, vol. 102, No. 1, p. 18003.DOI: 10.1209/0295-5075/102/18003

[8] N. I. Landy, S. Sajuyigbe, J. J. Mock, D. R. Smith, and W. J. Padilla, "Perfect metamaterial absorber," *Physical review letters,* 2008, vol 100, No. 20, p. 207402. DOI: 10.1103/PhysRevLett.100.207402

[9] A. Singh, A. Raj, A. Gupta, A. Tiwari and P. Kumar, "Split ring resonator biosensor-an innovative design and analysis", *2020 IEEE 8th International Conference on Photonics (ICP)*, Kota Bharu, Malaysia, 2020, pp. 117-118. DOI:10.1109/ICP46580.2020.9206451

[10] L. La Spada, F. Bilotti, and L. Vegni, "Metamaterial biosensor for cancer detection," *SENSORS, 2011 IEEE*, Limerick, Ireland, 2011, pp. 627-630. DOI: 10.1109/ICSENS.2011.6127103

[11] F. Lan, F. Luo, P. Mazumder, Z. Yang, L. Meng, Z. Bao, J. Zhou, Y. Zhang, S. Liang, Z. Shi, AR. Khan, Z. Zhang, L. Wang, J. Yin, and H. Zeng, "Dual-band refractometric terahertz biosensing with intense wave-matter-overlap microfluidic channel," *Biomedical Optics Express*, 2019, vol. 10, No. 8. pp. 3789-3799. DOI: doi.org/10.1364/BOE.10.003789

[12] M. Y. Azab, M. F. O. Hameed, A. M. Nasr and S. S. A. Obayya, "Highly sensitive metamaterial biosensor for cancer early detection," *IEEE Sensors Journal*, 2021, vol. 21, No. 6, pp. 7748-7755. DOI:10.1109/JSEN.2021.3051075

[13] A. S. Saadeldin, M. F. O. Hameed, E. M. A. Elkaramany and S. S. A. Obayya, "Highly sensitive terahertz metamaterial sensor," *IEEE Sensors Journal*, 2019, vol. 19, No. 18, pp. 7993-7999. DOI: 10.1109/JSEN.2019.2918214

[14] M. M. Hassan, F. S. Sium, F. Islam, S. M. Choudhury, "A review on plasmonic and metamaterial based biosensing platforms for virus detection," *Sensing and Bio-Sensing Research*, 2021, vol. 33, p. 100429. DOI: 10.1016/j.sbsr.2021.100429

[15] N. Akter, M. M. Hasan, N. Pala, "A review of THz technologies for rapid sensing and detection of viruses including SARS-CoV-2," *Biosensors*, 2021, vol. 11, No. 10, p. 349. DOI: 10.3390/bios11100349

[16] J. T. Hong, S. W. Jun, S. H. Cha, J. Y. Park, S. Lee, G. A. Shin, and Y. H. Ahn, "Enhanced sensitivity in THz plasmonic sensors with silver nanowires. *Scientific reports*, 2018, vol. 8, No. 1, p.15536. DOI:10.1038/s41598-018-33617-2

[17] D. K. Lee, J. H. Kang, J. Kwon, J. S. Lee, S. Lee, D. H. Woo, J. H. Kim, C. S. Song, Q. H. Park and M. Seo, "Nano metamaterials for ultrasensitive Terahertz biosensing," *Scientific reports*, 2017, vol. 7, No.1, p. 8146. DOI: 10.1038/s41598-017-08508-7

[18] A. Kovačević, M. Potrebić, and D. Tošić, "Sensitivity characterization of multi-band THz metamaterial sensor for possible virus detection," *Electronics*, 2022, vol. 11, No. 5, p. 699. DOI:10.3390/electronics11050699

[19] C. Tan, S. Wang, H. Yang, Q. Huang, S. Li, X. Liu, H. Ye, G. Zhang, "Hydrogenated Boron Phosphide THz-Metamaterial-Based Biosensor for Diagnosing COVID-19: A DFT Coupled FEM Study," *Nanomaterials*, 2022, vol. 12, No. 22, p. 4024. DOI:10.3390/nano12224024

[20] A. Keshavarz and Z. Vafapour, "Sensing avian influenza viruses using terahertz metamaterial reflector," *IEEE Sensors Journal*, 2019, vol. 19, No. 13, pp. 5161-5166. DOI: 10.1109/JSEN.2019.2903731

[21] Cao, Y., Nallappan, K., Guerboukha, H., Gervais, T., & Skorobogatiy, M. (2019). Additive manufacturing of resonant fluidic sensors based on photonic bandgap waveguides for terahertz applications. *Optics Express*, *27*(20), pp. 27663-27681. DOI: 10.1364/OE.27.027663

[22] Nickpay, M. R., Danaie, M., & Shahzadi, A. (2022). Highly sensitive THz refractive index sensor based on folded split-ring metamaterial graphene resonators. *Plasmonics*, *17*(1), pp. 237-248. DOI:10.1007/s11468-021-01512-8

[23] Razani, A. N., Rezaei, P., Zamzam, P., Khatami, S. A., & Daraei, O. M. (2022). Absorption-based ultra-sensitive RI sensor based on the flower-shaped graphene resonator for early detection of cancer. *Optics Communications*, *524*, 128775. DOI:10.1016/j.optcom.2022.128775

[24] Tammam, M. M. E., Hameed, M. F. O., Elkaramany, E. M., Ali, T. A., & Obayya, S. S. A. (2025). Versatile terahertz metamaterial sensor for biomedical applications. *Plasmonics*, *20*(5), pp. 2815-2828. DOI:10.1007/s11468-024-02401-6

[25] Z. Hafdi, Z. Mezache, J. Tao, and G. Guergour, "Analysis of Graphene Pythagoras Tree Fractal Antenna with Thin SiO Substrate in Terahertz Regime," *Annals of West University of Timisoara-Physics*,2023, vol. 65, pp. 1-11. DOI:10.2478/awutp-2023-0001

[26] Z. Mezache, Z. Hafdi, J. Tao, "Design of a novel graphene buzzle metamaterial refractometer for sensing of cancerous cells in the terahertz regime," *Optik*, 2023, vol. 287, p. 171170. DOI:10.1016/j.ijleo.2023.171170